**IEA Wind Task 46
Erosion of wind turbine blades**

Atmospheric drivers of wind turbine blade leading edge erosion: Ancillary variables

Technical report

Technical Report

Atmospheric drivers of wind turbine blade leading edge erosion: Ancillary variables

Prepared for the
International Energy Agency Wind Implementing Agreement

Prepared by
IEA Task 46, Workpackage #2

Lead author:
Sara C. Pryor (Cornell University)*
* correspondence to; sp2279@cornell.edu
Co-authors:
Rebecca J. Barthelmie (Cornell University)
Sergio Campobasso (Lancaster University)
Ebba Delwik (DTU)
Asta Hannisdottir (DTU)
Charlotte Hasager (DTU)
Stephan T. Kral (University of Bergen)
Joachim Reuder (University of Bergen)
Marianne Rodgers (WEICan)
Marijn Veraart (Ørsted)

Date: 15 March 2023

Purpose

Leading edge erosion (LEE) of wind turbine blades has been identified as a major factor in decreased wind turbine blade lifetimes and energy output over time. Accordingly, the International Energy Agency Wind Technology Collaboration Programme (IEA Wind TCP) created Task 46 to undertake cooperative research in the key topic of blade erosion.

This report is a product of WorkPackage 2 **Climatic conditions driving blade erosion.** The objectives of the work summarized in this report are to:

- Summarize efforts to elucidate critical atmospheric co-stressors that may accelerate leading edge erosion and hence for which meta-data regarding observations should be collated.
- Briefly describe and summarize additional data pertaining to those LEE co-stressors from sites that were the focus of analyses of hydrometeors in the report "Atmospheric drivers of wind turbine blade leading edge erosion: Hydrometeors" (Pryor et al. 2021)

Accompanying this report is a detailed spreadsheet that summarizes the meta-data regarding these co-stressor variables. That file is entitled: IEA46_WP2_METDATA_AncillaryData.xlsx. The doi is 10.5281/zenodo.7734765.

This report is released for public dissemination.

IEA Wind Task 46 Participants during period 2021-2025

Country	Contracting Party	Active Organizations
Belgium	Belgian Ministry of Economy	Engie
Canada	Natural Resources Canada	WEICan
Denmark	Danish Energy Agency	DTU (co-OA), Hempel, Ørsted A/S
Finland	Business Finland	VTT (co-OA)
Germany	Federal Ministry for Economic Affairs and Energy	Fraunhofer IWES, Covestro, Emil Frei (Freilacke), Nordex Energy SE, Mankiewicz, DNV
Ireland	Sustainable Energy Authority of Ireland	IT Carlow, NUI Galway, University of Limerick
Japan	New Energy and Industrial Technology Development Organization	AIST, Asahi Rubber Inc., Osaka University, Tokyo Gas Co.
the Netherlands	Netherlands Enterprise Agency	Eneco, TU Delft, Suzlon, TNO
Norway	Norwegian Water Resources and Energy Directorate	Equinor Energy AS, University of Bergen
Spain	CIEMAT	CENER, Aerox Advanced Polymers, CEU Cardenal Herrera University, Siemens Gamesa Renewable Energy, Nordex Energy Spain
United Kingdom	Offshore Renewable Energy Catapult	ORE Catapult, University of Bristol, University of Lancaster, Imperial College, Vestas
United States	U. S. Department of Energy	Cornell University, Sandia National Laboratories, 3M

Table of Contents

List of Figures

List of Tables

Executive Summary

Wind turbine blade leading edge erosion is, to the first order, the result of material stresses caused by kinetic energy transfer from hydrometeors impacting on the rotating blade. However, additional properties of the atmosphere can accelerate the progress of material damage. Thus, this report summarizes (1) efforts to elucidate key co-stressors and (2) develop meta-data for those atmospheric properties at sites that form the basis of ongoing research within the IEA Wind Technology Platform Task 46. The reader is directed to the World Meteorological organization activity area on Instruments and Methods of Observation Programme (IMOP) (https://community.wmo.int/en/activity-areas/imop) for further information regarding technical standards, quality control procedures and technical information about atmospheric measurement technologies (World Meteorological Organization 2021).

1   Introduction

Task 46 was established by the IEA Wind Technology Collaboration Programme (TCP), to achieve a better understanding of the key technical challenges within wind turbine blade leading edge erosion. It is aligned with two research priorities established by IEA TCP Wind, site characterization and advanced technology. The Task work plan is structured in four technical work packages (WP2-WP5) supported by a management work package (WP1).

This report is a product of WorkPackage 2 **Climatic conditions driving blade erosion.** It follows from an earlier report and scholarly publication (Pryor et al. 2022; Pryor et al. 2021) that:

1) Describes hydroclimatic conditions at key sites with high wind energy potential of installed capacity and contextualizes those measurements in the broader literature.
2) Describes metrologies for hydroclimatic measurements and compares and contrasts those measurement technologies.
3) Summarizes closure experiments among ground-based and remote sensing disdrometers (devices that measure hydrometeor size distributions).
4) Assesses the degree to which observed droplet size distributions fit commonly used hydrometeor size distribution approximations.

Table 1: Summary of the locations from which data have been reported in IEA Task46 WP2. Sites shown in black are as in the first Deliverable (earlier report and scholarly publication (Pryor et al. 2022; Pryor et al. 2021)). An additional site that has been added and will replace Coastal Uk (Weybourne) henceforth is shown in red.

Location label used here	Site	Latitude	Longitude	Instrument type used for droplet size distribution measurements
US SGP	DoE ARM, Lamont, SGP, USA	36.6072ºN	97.4875ºW	OTT Parsivel[2], 2D Video, Impact
US NE	*Cornell University, New York, USA*	*42.4534ºN*	*76.4735ºW*	*4 × OTT Parsivel[2]*
Canada coastal	WEICan, Canada	47.035ºN	64.015ºW	CSI PWS100
Coastal UK	Weybourne Atmospheric Observatory, UK	52.9433ºN	1.1414ºE	Thies LPM
Norway coastal	Bergen, Norway	60.38ºN	5.33ºE	OTT Parsivel[2,] MRR
North Sea	Horns Rev, Denmark	55.6ºN	7.59ºE	OTT Parsivel[2]
Denmark inland	DTU, Denmark	55.693ºN	12.1ºE	Thies LPM, OTT Parsivel[2]
UK inland	Lancaster, UK	54.0449ºN	2.7993ºE	CSI PWS100 + Theis LPM

Note: The US NE site was used for a disdrometer closure experiment but is not a core location for ongoing analyses.

Wind turbine blade leading edge erosion is, to the first order, the result of material stresses causes by kinetic energy transfer from hydrometeors impacting on the rotating blade. However, additional properties of the atmosphere can accelerate the progress of material damage such as solar radiation exposure (UV, ultra-violet radiation degradation), impacts of/corrosion from airborne particles such as dust or sea-salt, exposure of the

blades to low temperatures or cycling of thermal expansion and contraction, and unbalanced rotation and excess vibration due to uneven ice accumulation (Afzal and Virk 2018; Brøndsted et al. 2005; Godfrey et al. 2021; Keegan et al. 2013; Law and Koutsos 2020; Pathak et al. 2022; Rizk et al. 2020). This report summarizes (1) efforts to elucidate key-co-stressors for which atmospheric observations are available and (2) develop meta-data for those atmospheric properties.

2 Co-stressors: Survey

During 2022 an informal survey was sent by the WP2 participants to other workpackages within the IEA TCP task 46 that comprised 6 sheets within a Microsoft PowerPoint file. Those sheets as provided in Figure 1 and the responses to that survey are summarized in Table 2.
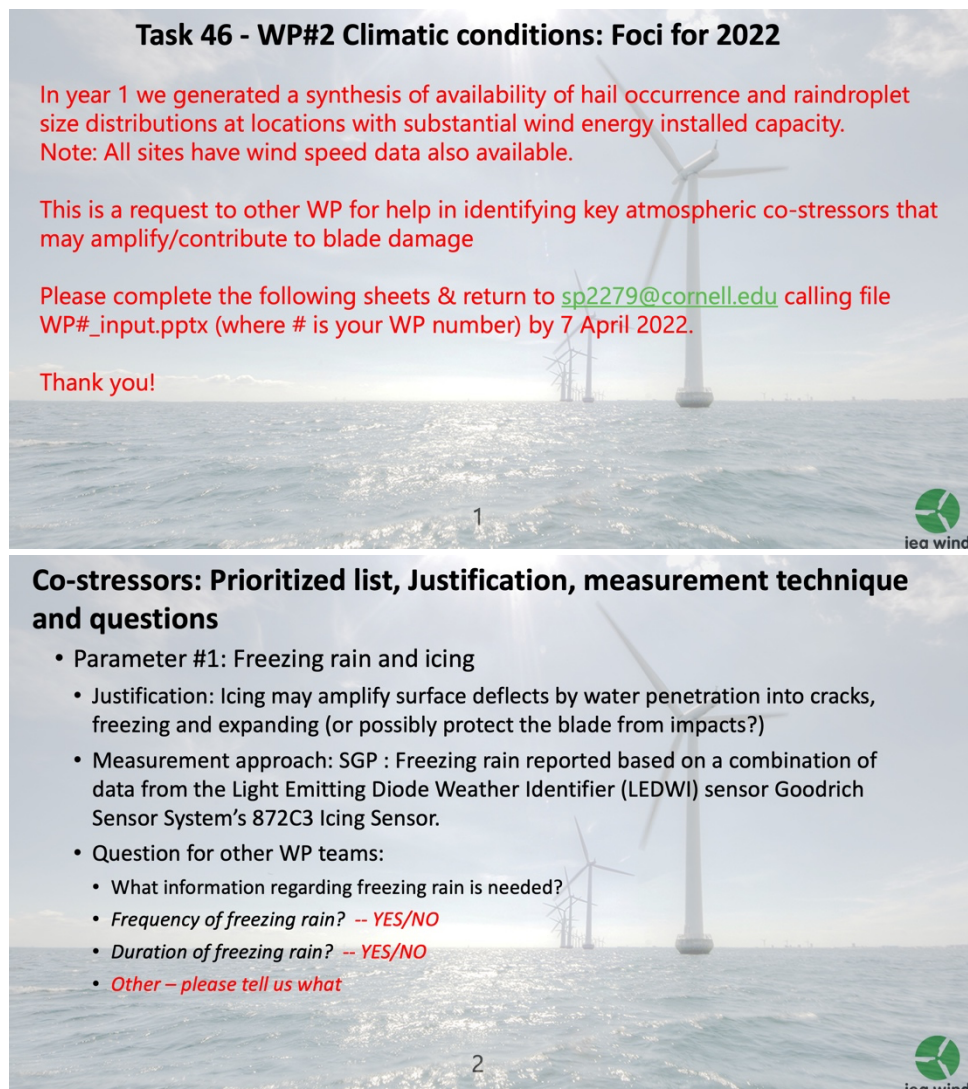
Co-stressors: Prioritized list, Justification, measurement technique and questions

- Parameter 2: UV receipt
  - Justification: already part of the DNV/GL materials consideration for materials degradation
  - Measurement approach: SGP: Sun-photometer & pyranometers measure downwelling radiation <please fill in how/if UV is measured at your site>
  - Question for other WP teams:
    - What information regarding UV receipt is needed?
    - *Specific wavelengths? -- YES/NO*
    - *Annual total downwelling shortwave radiation accumulation? (i.e. sum of W/m^2) -- YES/NO*
    - *Other – please tell us what*

3

Co-stressors: Prioritized list, Justification, measurement technique and questions

- Parameter 3: Temperature variability
  - Justification: Materials expansion/contraction may amplify surface defects
  - Measurements: e.g. SGP: many thermometers + microwave thermal profilers.
  - Question for other WP teams:
    - What information regarding temperature range is needed?
    - *Mean diurnal amplitude? -- YES/NO*
    - *Mean seasonal amplitude? -- YES/NO*
    - *Other – please tell us what*

4

Co-stressors: Prioritized list, Justification, measurement technique and questions

- Parameter 4: Aerosols (wind blown dust & sea spray)
  - Justification: POSSIBLY sand blasting of blades (SGP? China/India) &/or **chemical corrosion (wider geographic range of importance?)**. We are uncertain how often these aerosols are lofted into the rotor plane. GE make a specific WT for dust rich locations - is it an issue for LEE?
  - Measurement: SGP: Nephelometer + size distributions of fine aerosols (SMPS) – but otherwise very few available for other sites.
  - Question for other WP teams:
    - Does you believe we need aerosol measurements? If so what types?
    - *$PM_{2.5}$ or PM_{10} mass? -- YES/NO*
    - *Composition? -- YES/NO*
    - *Other – please tell us what….*
    - *Note: We are very unclear direct measurements will be possible but we could use reanalyses.*

5
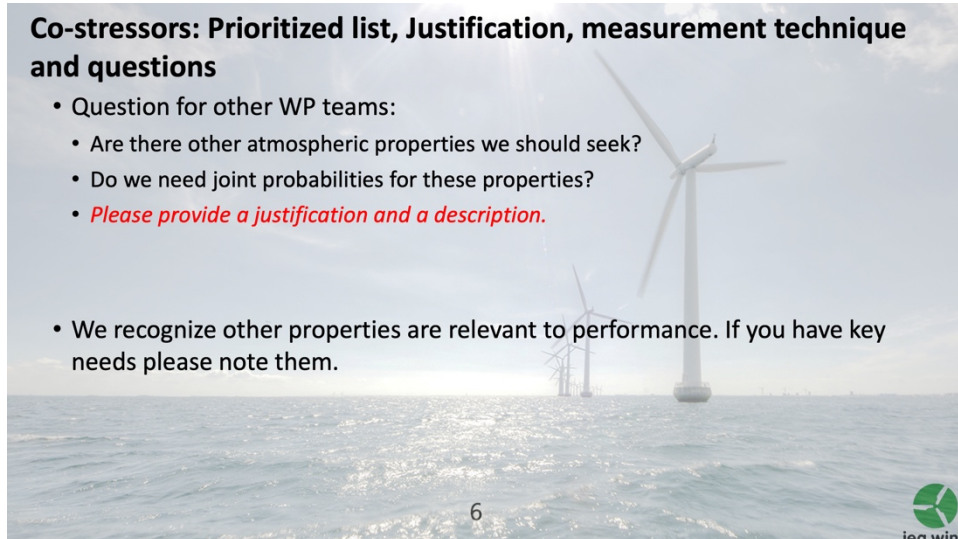
Figure 1: Survey sent to other IEA Task 46 workpackages regarding the relative importance of LEE co-stressors

Table 2: Survey responses indicating how many of the other three Task 46 workpackages identified the specified variable as of key importance to leading edge erosion and a summary narrative of comments received.

Variable	Importance (# of positive responses from the 3 WPs)	Described variable	Narrative
Wind speed	Essential to closing velocity between hydrometeor and blade (3)	Weibull distribution parameters at/close to wind turbine hub-height	
Freezing rain & icing	1	Frequency and duration	Challenging to measure and not included in WP5 modelling.
Solar radiation	Very important (3)	Annual total downwelling shortwave radiation	Included in WP5 in terms of polymer chemistry linked with erosion performance.
Temperature variability	Very important (3)	Diurnal amplitude and seasonal amplitude	Included in WP5 in terms of viscoelasticity relation with erosion mechanics.
Aerosols	1	pH/salinity and size distribution	Possible pH/salinity may be important from chemical corrosion perspective and/or mechanical erosion due to sand blasting on a local scale in some environments. But due to a lack of consistent measurements this is not a priority.

Informed by these survey responses *AND* information regarding access to observational data regarding these variables, a decision was taken to compile meta-data regarding the instrumentation used and data availability for the parameters listed below for the seven primary focal sites for WP2 that are summarized in Table 1.

3   Co-stressors: Description and Metadata

3.1 Downwelling solar radiation

There are multiple metrologies available for measurement of downwelling solar radiation (World Meteorological Organization 2021) including:
1) Pyranometer: Measurement of global solar radiation (all wavelengths) over a hemispheric field of view.
2) Photometer: Measurement of only the visible part of the spectrum over a hemispheric field of view. Sun-photometers may also be employed that track the position of the Sun.

Here we consider total downwelling shortwave (SW) radiation which is dominated by wavelengths (λ) ~ 0.29 to 3 μm. Indeed 97% of solar energy at the top of Earth's atmosphere falls into this spectral range (World Meteorological Organization 2021). Radiation with λ > 700 nm is referred to as Infrared, that with λ between 400 nm and 700 nm is described as Visible. Radiation with λ < 400 nm (0.4 μm) is referred to as ultraviolet radiation (UV) and is sometimes divided into (World Meteorological Organization 2021):
- UV-A: 315-400 nm
- UV-B: 280-315 nm
- UV-C: 100-280 nm

Approximately 9% of radiation emission from the Sun lies within the UV wavelengths, 39% in the Visible wavelengths and 53% in IR wavelengths (Frederick et al. 1989). The UV flux is strongly absorbed by Earth's atmosphere. No measurable UV-C ever reaches Earth's surface due to very strong atmospheric attenuation largely due to absorption by molecular oxygen and ozone. UV-B is also strongly attenuated by the atmosphere and is strongly absorbed by ozone. Hence, 95% of UV that reaches Earth's surface is in the UV-A waveband (Frederick et al. 1989).

The primary reason for inclusion of downwelling solar radiation in this co-stressor summary is that UV degradation of polyurethane coatings has been documented (Mayer et al. 2022). There is some evidence UV-A (wavelengths (λ) = 320 and 400 nm) is the most important contributor to blade coating degradation (i.e. is more damaging than radiation with longer wavelengths) (Keegan et al. 2013). However, wavelength specific measurements of downwelling solar radiation are relatively sparse. Thus, here we use total downwelling shortwave radiation as a proxy for UV.

These radiation data are summarized here using the following method: The radiation flux (in Watts per meter-squared, Wm^{-2}) in each measurement period (e.g. each hour) are averaged to generate a MEAN value. This is then multiplied by 365 (number of days in a year) $\times$ 24 (hours in a day) $\times$ 60 (minutes in a hours in a day) $\times$ 60 (seconds in a minute) to yield a mean annual receipt in Jm^{-2} per year.

3.2 Temperature variability

There are multiple metrologies being deployed to make measurements of near-surface temperature. While the majority of early measurements relied on expansion of a liquid (e.g. mercury in glass thermometers) most thermometers now employ technologies reliant on measurement of radiation (infrared thermometers) or, more commonly, electronic thermometers that work on the principle that the resistance or conductance of electrical energy through a wire is a function of the temperature of the wire (Burt and de

Podesta 2020; World Meteorological Organization 2021). PT 100 temperature sensors are the most common type of platinum resistance thermometer. WMO recommendations indicate thermometer measurements should be taken at a height of 1.25 and 2 m above the ground, preferably over a natural surface (e.g. grass) and that thermometers should be ventilated and properly screened to avoid heating due to radiation exposure (World Meteorological Organization 2021).

There are two principal reasons for inclusion of air temperature variability in these meta-data analysis of co-stressors. First, theoretical and experimental work has indicated that low temperatures degrade the erosion performance of polyurethane protective leading-edge coatings (Godfrey et al. 2021). Second, thermal cycling (expansion and contraction of the blades) is an important source of materials wear (Lachenal et al. 2013).

In the meta-data summary, the air temperature measurements are summarized in terms of the mean diurnal temperature range and the mean seasonal variability. The following procedures are applied to observations taken with either a 10-minute or hourly averaging period:

- The mean diurnal temperature range is approximated as the difference between the mean daily maximum temperature (Tmax) and the corresponding mean daily minimum temperature (Tmin) in each calendar month.
- The seasonal variability is represented as the difference in mean daily Tmax (or mean daily Tmin) in the calendar month with highest values minus the mean Tmax (or mean daily Tmin) in the calendar month with lowest values.

3.3 Wind speeds

There are multiple metrologies being applied for wind speed measurements including cup-anemometers that work by harnessing the momentum in the air (World Meteorological Organization 2021), sonic anemometers that measures variations in the transmission of ultrasonic pulses (sound waves) (Technical Committee ISO/TC 146 2002), and lidars that use Doppler frequency shifts in the emitted laser beam (Wang et al. 2015; Wang et al. 2016a; Wang et al. 2016b). Many of these technologies have been extensively evaluated in Wind Technology Collaboration Programme Tasks 52 https://iea-wind.org/task52/ (previously Task 32) and Task 17 Data Base on Wind Characteristics.

There are two principal reasons for inclusion of information about the wind speed probability distribution in this co-stressor analysis. First and foremost, wind speeds at hub-height are the single most important determinant of the closing velocity between falling hydrometeors and the blade leading edge. Hydrometeors have typical terminal fall velocities of upto 8 ms^{-1} (see Figure 2 reproduced from (Pryor et al. 2021)), while at rated speed the tip speed of a typical wind turbine as 60-100 ms^{-1} (see Figure 3 reproduced from (Pryor et al. 2021)). The probability distribution describes the likelihood of the wind turbine being at rated speed and thus rotating at the maximum speed. Second, flow variability is a major source of mechanical loads on the blades.

Wind speed data are summarized by fitting the sub-hourly or hourly values to a two-parameter Weibull distribution using maximum likelihood methods and reporting the scale and shape distribution parameters (*A* and *k*) (Pryor et al. 2004; Wilks 2011). The probability distribution (i.e. probability of a wind speed, WS, of a given magnitude) is given by:

$$f(WS) = \frac{k}{A}\left(\frac{WS}{k}\right)^{k-1} exp\left[-\left(\frac{WS}{A}\right)^{k}\right] \tag{1}$$

While the cumulative probability distribution (the total probability of observing of value equal to or less than that specified) is given by:

$$F(WS) = 1 - exp\left[-\left(\frac{WS}{A}\right)^{k}\right] \tag{2}$$
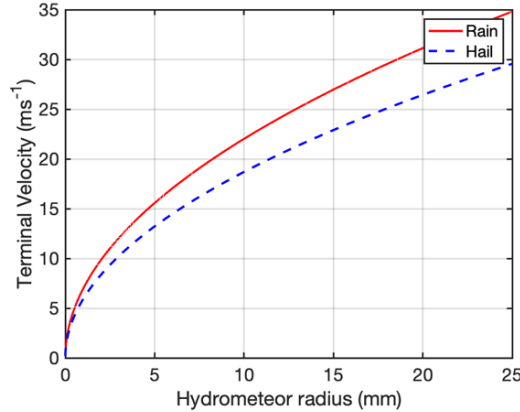
Figure 2 Terminal fall velocities for rain droplets and hail under the following assumptions: ρ_o= 1.225 kgm^{-3}, ρ_{air}=0.999*ρ_o , ρ_i = 900 kgm^{-3}.
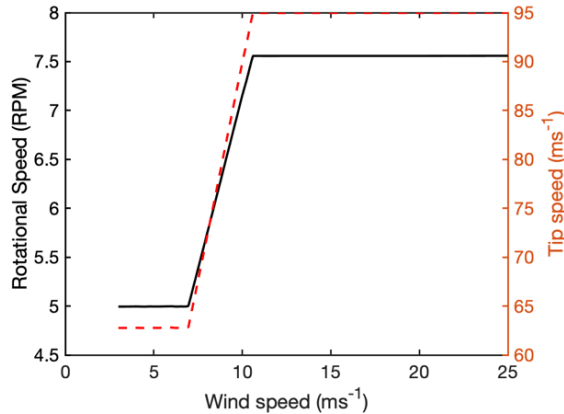
Figure 3 Illustrative example of wind turbine RPM and tip speed as a function of wind speed for the IEA 15 MW reference turbine (Gaertner et al. 2020). Power production begins at 4 ms^{-1} and ceases at wind speeds > 25 ms^{-1}, thus no RPM or tip-speed data are plotted for wind speeds outside of the range of 4-25 ms^{-1}.

3.4 Other parameters

While estimates for aerosol characteristics (mass abundance, chemical composition and size distribution) and for the occurrence and magnitude of icing at not available at the majority of the sites that form the focus on IEA Task46 WP2 activities, it is worthy of note that such measurements are available at the US SGP DoE ARM facility. Thus, it may be fruitful for future research to use the SGP for a comprehensive analysis of damage mechanisms resulting in leading edge erosion.

3.5 Modeled estimates for co-stressors

Data for the three critical co-stressors described above have also been summarized at each of our focus seven of study locations using output from the ERA5 reanalysis (Hersbach et al. 2020). For the European sites data from the NORA3 hindcast (Haakenstad et al. 2021) are also summarized. While such estimates are clearly of lower value than direct observations due to their higher uncertainty and relatively coarse spatial and temporal scales, where observational data are lacking they may provide first order estimates for some properties of interest. The data summaries also allows a very preliminary assessment of these model products for some of these key co-stressor variables.

Consistent with previous research summarized in the literature that has illustrated higher fidelity of ERA5 relative to past reanalysis products (He et al. 2021; Urraca et al. 2018), results for downwelling solar radiation exhibit good agreement between estimates from in situ measurements and ERA5. At sites examined herein, value from the reanalyses and the observations lie within 3.5% of each other. ERA5 does not assimilate land surface temperatures but does assimilate near-surface air temperature observations. Accordingly, consistent with previous literature (Boettcher et al. 2023; Martens et al. 2020), ERA5 appears to be a credible source of air temperatures at the sites considered herein in terms of characterization of the seasonal cycle of Tmin and Tmax (see example in Figure 4).

Much lower degree of overall agreement is found for wind speeds from ERA5 and NORA3 at the focus sites relative to direct observations (see discussion in (Pryor et al. 2022; Pryor et al. 2021)). This is consistent with the literature that has shown wind speeds from ERA5 exhibit spatial varying fidelity relative to observations (Jourdier 2020; Pryor et al. 2020). This is likely due to unpresented sub-grid scale orographic variability, land surface variability, spectral truncation, and the spatial variability in wind speed data available for assimilation into the reanalysis model. Given the importance of small variations in hub-height wind speeds to rotor rotational speed (Figure 3) the authors urge great caution be used in employing these modeled estimates in leading edge erosion studies.
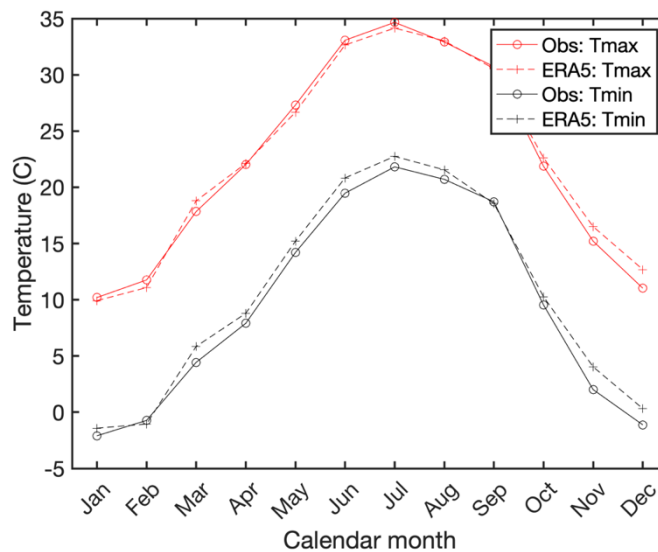

Figure 4: Mean monthly Tmax and Tmin for the ERA5 grid cell containing SGP Lamont and from direct observations for 2017-2021.

15

Table 3: Summary of ancillary properties from measurements: Mean difference in the monthly mean Tmax and Tmin (deg C), diurnal variability of temperature (DTR = Diurnal temperature range; daily Tmax – Tmin averaged) (deg C) and total <u>annual</u> SW radiation receipt (Jm^{-2})

Location label used here	Site	Seasonal Difference: Month with highest Tmax minus month with lowest Tmax	Seasonal Difference: Month with highest Tmin minus month with lowest Tmin	Mean DTR	Total SW radiation (Jm^{-2} per year)
US SGP	DoE ARM, Lamont, SGP, USA	24.5	23.9	12.9	6.02×10^9 (from observations)
Canada coastal	WEICan, Canada	27.5	26.6	5.7	5.1×10^9 (from ERA5)
Coastal UK	Weybourne Atmospheric Observatory, UK	11.2 (ERA5)	11.2 (ERA5)	6.5 (ERA5)	4.131×10^9 (from ERA5)
Norway coastal	Bergen, Norway	11.7	5.7	6.0	3.27×10^9 (from ERA5)
North Sea	Horns Rev, Denmark	13.6 (ERA5)	13.7 (ERA5)	2.2	4.131×10^9 (from ERA5)
Denmark inland	DTU, Denmark	18,4	14.5	5.9	3.78×10^9 (from observations)
UK inland	Lancaster, UK	11.9	9.8	5.6	3.35×10^9 (from observations)

Table 4: Summary of ancillary properties from measurements: Wind parameters

Location label used here	Site	Weibull A (ms^{-1})	Weibull k	Instrument type used for measurements
US SGP	DoE ARM, Lamont, SGP, USA	8.96	2.18	Doppler lidar at height = 90 m.
Canada coastal	WEICan, Canada	10.3	2.00	Cup anemometer at height = 80 m
Coastal UK	Weybourne Atmospheric Observatory, UK	10.06	2.3	No observations available. NORA3 given for height = 100 m
Norway coastal	Bergen, Norway	7.09	1.73	No observations available. NORA3 given for height = 100 m
North Sea	Horns Rev, Denmark	11.04	2.3	No observations available. NORA3 given for height = 100 m
Denmark inland	DTU, Denmark	8.12	2.35	Cup anemometer at a height of 94 m, 2017-2021
UK inland	Lancaster, UK	11.15	2.17	No observations available at hub-height. NORA3 given for height = 100 m

Reanalysis products also include hydroclimate parameters. However, they generally only report rainfall rates (typically at hourly resolution). As described in detail in previous products of this WorkPackage once-hourly rainfall rates are not adequate for assessing potential material damage because of three linked factors:

1) Precipitation rates (i.e. the rate of accumulation of liquid water at the surface, usually

expressed in mmhr^{-1}) are highly dependent on the sampling interval (see Figure 5c). At the US SGP site, 10% of rainfall rates averaged over 1 minute have an intensity of > 4.5 mmhr^{-1}. When the data are averaged over 10 minutes, this 90th percentile value (i.e. the value exceeded in 10% of periods with precipitation) drops to 2.2 mmhr^{-1}. As shown in Figure 5a, the total number concentration of hydrometeors increases with precipitation intensity and the number of large droplets increases by a factor of over five for rainfall rates of 6-11 mmhr^{-1} versus 2-3 mmhr^{-1}.

2) There is no universal function that links precipitation rates to hydrometeor size distribution and number concentrations. As shown in Figure 5b the number weighted mass mean diameter (D_m), which is a metric of the droplet size distribution, varies over an order of magnitude in different events with the same rainfall rate.

3) The mass of hydrometeors and the kinetic energy exchanged during their impacts on the blade are a nonlinear function of hydrometeor diameter. Thus, the presence of a few larger hydrometeors is critical to the total kinetic energy of impacts.

The fidelity of rainfall rates from reanalysis products is lower than that for air temperatures. Thus while ERA5 is widely recognized as exhibiting higher fidelity than previous generation reanalyses with respect to precipitation, that fidelity is highly spatially and temporally variable and is less good for shorter sampling periods than in the annual mean (Hassler and Lauer 2021; Lavers et al. 2022; Tarek et al. 2020). For these reasons, rainfall rates from reanalysis products are not sufficient for computing material damage and wind turbine blade leading edge erosion. Preference should be given to in situ measurements of wind speed and droplet size distributions collected at high temporal resolution.
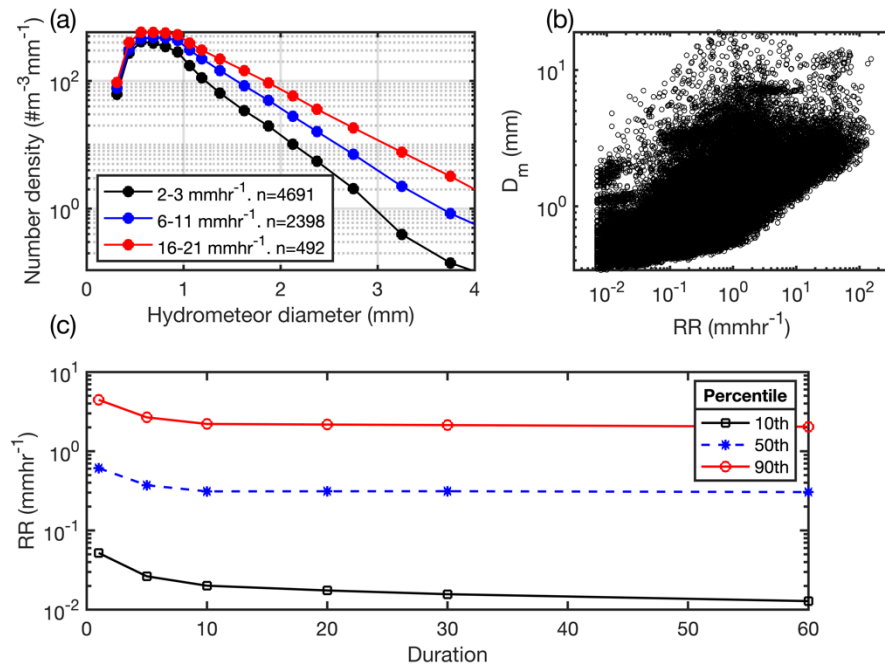

Figure 5: (a) Mean droplet size distributions for different rainfall rate classes (RR); 2–3 mmhr^{-1}, 6–11 mmhr^{-1} and 16–21 mmhr^{-1}. The legend shows the number of 1 min periods (n) in each class. (b) Scatterplot of 1 min RR versus the mass-weighted droplet mean diameter (D_m). (c) 10th, 50th and 90th percentile rainfall rate (RR, in mmhr^{-1}) as a function of averaging period. All analyses based on 1-minute data collected with an OTT Parsivel^2 disdrometer at the US SGP site conditionally sampled for liquid only precipitation (Figure adapted from two figures presented in (Pryor et al. 2022)).

4 Overview of the metadata structure

The tabs in the EXCEL spreadsheet; IEA46_WP2_METDATA_AncillaryData.xlsx denote the different sites with the tabs specifying the site using the 'Location label used here' definitions from Tables 2-4. In each tab, the upper rows describe the site location, period for which hydrometeor data are available and then the availability of measurements of the co-stressors from observations. Then observational values are reported. Below these are reports of wind, solar radiation and temperature output from ERA5 and for some locations in Europe from NORA3. These analyses are presented for a twenty-year period (1992-2021) and also for a short period (2017-2021) that typically corresponds to the period for which the disdrometer data are available.

5 References

Afzal, F., and M. S. Virk, 2018: Review of icing effects on wind turbine in cold regions. *E3S web of conferences*, EDP Sciences, 01007.

Boettcher, M., M. Röthlisberger, R. Attinger, J. Rieder, and H. Wernli, 2023: The ERA5 extreme seasons explorer as a basis for research at the weather and climate interface. *Bulletin of the American Meteorological Society*, **In press**.

Brøndsted, P., H. Lilholt, and A. Lystrup, 2005: Composite materials for wind power turbine blades. *Annu. Rev. Mater. Res.*, **35,** 505-538.

Burt, S., and M. de Podesta, 2020: Response times of meteorological air temperature sensors. *Quarterly Journal of the Royal Meteorological Society*, **146,** 2789-2800.

Frederick, J., H. Snell, and E. Haywood, 1989: Solar ultraviolet radiation at the earth's surface. *Photochemistry and photobiology*, **50,** 443-450.

Gaertner, E., and Coauthors, 2020: IEA Wind TCP Task 37: Definition of the IEA 15-Megawatt Offshore Reference Wind Turbine. National Renewable Energy Lab.(NREL), Golden, CO (United States). Available for download from: https://www.osti.gov/biblio/1603478, 44 pp.

Godfrey, M., O. Siederer, J. Zekonyte, I. Barbaros, and R. Wood, 2021: The effect of temperature on the erosion of polyurethane coatings for wind turbine leading edge protection. *Wear*, **476,** 203720.

Haakenstad, H., Ø. Breivik, B. R. Furevik, M. Reistad, P. Bohlinger, and O. J. Aarnes, 2021: NORA3: A nonhydrostatic high-resolution hindcast of the North Sea, the Norwegian Sea, and the Barents Sea. *Journal of Applied Meteorology and Climatology*, **60,** 1443-1464.

Hassler, B., and A. Lauer, 2021: Comparison of reanalysis and observational precipitation datasets including ERA5 and WFDE5. *Atmosphere*, **12,** 1462.

He, Y., K. Wang, and F. Feng, 2021: Improvement of ERA5 over ERA-Interim in simulating surface incident solar radiation throughout China. *Journal of Climate*, **34,** 3853-3867.

Hersbach, H., and Coauthors, 2020: The ERA5 global reanalysis. *Quarterly Journal of the Royal Meteorological Society*, **146,** 1999-2049.

Jourdier, B., 2020: Evaluation of ERA5, MERRA-2, COSMO-REA6, NEWA and AROME to simulate wind power production over France. *Advances in Science and Research*, **17,** 63-77.

Keegan, M. H., D. Nash, and M. Stack, 2013: On erosion issues associated with the leading edge of wind turbine blades. *Journal of Physics D: Applied Physics*, **46,** 383001.

Lachenal, X., S. Daynes, and P. M. Weaver, 2013: Review of morphing concepts and materials for wind turbine blade applications. *Wind energy*, **16,** 283-307.

Lavers, D. A., A. Simmons, F. Vamborg, and M. J. Rodwell, 2022: An evaluation of ERA5 precipitation for climate monitoring. *Quarterly Journal of the Royal Meteorological Society*, **148,** 3152-3165.

Law, H., and V. Koutsos, 2020: Leading edge erosion of wind turbines: Effect of solid airborne particles and rain on operational wind farms. *Wind Energy*, **23,** 1955-1965.

Martens, B., D. L. Schumacher, H. Wouters, J. Muñoz-Sabater, N. E. Verhoest, and D. G. Miralles, 2020: Evaluating the land-surface energy partitioning in ERA5. *Geoscientific Model Development*, **13,** 4159-4181.

Mayer, P., M. Lubecki, M. Stosiak, and M. Robakowska, 2022: Effects of surface preparation on the adhesion of UV-aged polyurethane coatings. *International Journal of Adhesion and Adhesives*, **117,** 103183.

Pathak, S. M., and Coauthors, 2022: Solid particle erosion studies of ceramic oxides reinforced water-based PU nanocomposite coatings for wind turbine blade protection. *Ceramics International*, **48,** 35788-35798.

Pryor, S. C., F. W. Letson, and R. J. Barthelmie, 2020: Variability in wind energy generation across the contiguous USA. *Journal of Applied Meteorology and Climatology* **59,** 2021-2039.

Pryor, S. C., M. Nielsen, R. J. Barthelmie, and J. Mann, 2004: Can satellite sampling of offshore wind speeds realistically represent wind speed distributions? Part II: Quantifying uncertainties associated with sampling strategy and distribution fitting methods. *Journal of Applied Meteorology*, **43,** 739-750.

Pryor, S. C., and Coauthors, 2022: Atmospheric Drivers of Wind Turbine Blade Leading Edge Erosion: Review and Recommendations for Future Research. *Energies*, **15,** 8553, doi: 8510.3390/en15228553.

Pryor, S. C., and Coauthors, 2021: Atmospheric drivers of wind turbine blade leading edge erosion: Hydrometeors. Technical report from IEA Wind Task 46 Erosion of wind turbine blades, Technical report from IEA Wind Task 46 Erosion of wind turbine blades. 46 pp. Available for download from: https://iea-wind.org/task46/t46-results/.

Rizk, P., N. Al Saleh, R. Younes, A. Ilinca, and J. Khoder, 2020: Hyperspectral imaging applied for the detection of wind turbine blade damage and icing. *Remote Sensing Applications: Society and Environment*, **18,** 100291.

Tarek, M., F. P. Brissette, and R. Arsenault, 2020: Evaluation of the ERA5 reanalysis as a potential reference dataset for hydrological modelling over North America. *Hydrology and Earth System Sciences*, **24,** 2527-2544.

Technical Committee ISO/TC 146, 2002: Meteorology — Sonic anemometers/thermometers — Acceptance test methods for mean wind measurements, Available for pruchase from: https://www.iso.org/standard/29291.html.

Urraca, R., T. Huld, A. Gracia-Amillo, F. J. Martinez-de-Pison, F. Kaspar, and A. Sanz-Garcia, 2018: Evaluation of global horizontal irradiance estimates from ERA5 and COSMO-REA6 reanalyses using ground and satellite-based data. *Solar Energy*, **164,** 339-354.

Wang, H., R. J. Barthelmie, A. Clifton, and S. C. Pryor, 2015: Wind measurements from arc scans with Doppler wind lidar. *Journal of Atmospheric and Oceanic Technology* **32,** 2024-2040.

Wang, H., R. J. Barthelmie, S. C. Pryor, and G. Brown, 2016a: Lidar arc scan uncertainty reduction through scanning geometry optimization. *Atmospheric Measurement Techniques*, **9,** 1653-1669.

Wang, H., R. J. Barthelmie, P. Doubrawa, and S. C. Pryor, 2016b: Errors in radial velocity variance from Doppler wind lidar. *Atmospheric Measurement Techniques*, **9,** 4123-4139.

Wilks, D. S., 2011: *Statistical methods in the atmospheric sciences.* Vol. 100, Academic Press. ISBN: 9780123850225.

World Meteorological Organization, 2021: Guide to Instruments and Methods of Observation: Volume 1 - Measurement of Meteorological Variables, Geneva, Switzerland, 580 pp.